J Mater Sci (2008) 43:7331–7337
DOI 10.1007/s10853-008-2809-5

ULTRAFINE-GRAINED MATERIALS

Effect of strain on "hardening by annealing and softening by deformation" phenomena in ultra-fine grained aluminum

Daisuke Terada · Hironobu Houda · Nobuhiro Tsuji

Received: 7 March 2008 / Accepted: 16 June 2008 / Published online: 26 July 2008

Abstract Ultra-fine grained (UFG) metals fabricated by severe plastic deformation (SPD) sometimes exhibit peculiar mechanical properties. For example, the "hardening by annealing and softening by deformation" was reported in UFG aluminum, which was totally opposite to the behaviors of conventionally coarse-grained materials. In this study, the effect of SPD strain on the peculiar phenomena was investigated. The UFG aluminum was fabricated by various cycles of the accumulative roll-bonding (ARB) process with lubrication at ambient temperature. The specimen ARB-processed by ten cycles certainly showed the peculiar phenomena. On the other hand, the 6-cycle specimen did not show the phenomena but was softened by annealing and hardened by deformation normally. From the results of microstructural characterization, it was suggested that the difference in the change of the mechanical property during annealing and deformation between 6-cycle and 10-cycle specimens was caused by the difference in the grain size and/or the texture components, which depended on the SPD strain.

Introduction

It is well known that the ultra-fine grained (UFG) materials having the grain size <1 μm are fabricated by severe plastic deformation (SPD) processes [1–4]. The UFG materials sometimes show peculiar mechanical properties. For example, it was reported that the strength increased by annealing and decreased by subsequent deformation in the UFG aluminum fabricated by the accumulative roll-bonding (ARB) process, which was called "hardening by annealing and softening by deformation" [5]. Such phenomena were confirmed in UFG low-carbon steel as well [6]. The phenomena are completely opposite to the typical behavior of conventionally coarse-grained materials with grain size lager than several tens of micrometers. The phenomena were explained by the correlation between the strength and the density of dislocation sources in the nanostructured metals [5]. Firstly the dislocations are hard to be activated and multiplied within the ultrafine grains due to the small spaces. In the as-SPD processed materials, however, free dislocations as well as dislocation sources remain in the microstructure, which would make the yielding relatively easy. When the SPD specimens are annealed at low temperature where no recrystallization or no significant grain growth occurs, the free dislocations and dislocation sources are annealed out, resulting in "hardening."

However, the effect of microstructural parameters such as ultrafine grain size, dislocation density, textures, and fraction of low-angle boundaries on the unique phenomena has not been clarified in detail. The microstructural parameters greatly depend on the total strain applied during the SPD process. Therefore, in order to clarify the mechanism of the "hardening by annealing and softening by deformation" phenomena furthermore, the effect of the SPD strain on the phenomena was investigated in this study. The UFG specimens were fabricated by the ARB process by various strains. The specimens were annealed at a temperature lower than recrystallization temperature

D. Terada (✉) · H. Houda · N. Tsuji
Department of Adaptive Machine Systems, Graduate School of Engineering, Osaka University, Osaka 565-0871, Japan
e-mail: terada@ams.eng.osaka-u.ac.jp

H. Houda
e-mail: hironobu.houda@ams.eng.osaka-u.ac.jp

N. Tsuji
e-mail: tsuji@ams.eng.osaka-u.ac.jp

and subsequently deformed by rolling. The changes of mechanical properties caused by annealing and subsequent deformation were investigated. The microstructures of the UFG materials and the annealed UFG materials were also characterized, in order to get deeper understanding on the peculiar mechanical properties.

Experimental

A commercial purity aluminum (A1100, 99.11% purity) was used in this study. The chemical composition of the aluminum is shown in Table 1. UFG aluminum was fabricated by the ARB process [3]. Two initial sheets of 1-mm thick were stacked to 2-mm thick after degreasing and wire-brushing the contact surfaces, and then roll-bonded by 50% reduction in one pass at ambient temperature. The bonded sheet was cut in half-length in order to obtain two sheets having the same dimension as the initial specimen. Then, the sheets were provided for the surface treatments, stacking, and roll-bonding. These procedures were repeated up to six or ten cycles. The total equivalent strains corresponding to six and ten cycles were 4.8 and 8.0, respectively. The ARB process was carried out under well-lubricated condition using a two-high mill having a roll diameter of 310 mm. It should be noted that the ARB process in the previous study [5] where the peculiar phenomena were reported was carried out under high friction condition without lubrication. The roll peripheral speed was 0.29 m s^{-1}, so that the mean strain rate during rolling was 19 s^{-1}. The sheets were cooled into water immediately after roll-bonding.

The specimens ARB-processed by six and by ten cycles were annealed at 150 °C for 1.8 ks in the air. The annealed specimens were subsequently deformed by rolling with 15% reduction under the same conditions in the ARB process.

Tensile tests of the ARB specimen, the annealed specimen, and the subsequently deformed specimen were carried out. Specimens 5 mm in gage width and 10 mm in gage length (1/5 of JIS-5 specimen) were cut with an electric discharge machine and tested at an initial strain rate of 8.3×10^{-4} s^{-1} at ambient temperature. The tensile direction was parallel to the rolling direction (RD) of the sheets.

The microstructural characterization of the specimens was carried out by electron backscattering diffraction pattern (EBSD) measurement in a scanning electron microscope equipped with field emission-type gun (FE-SEM) and transmission electron microscopy (TEM). For EBSD measurement, the specimens perpendicular to transverse direction (TD) of the sheet were polished with sandpapers and then electro-polished in a 30 vol% HNO_3 + 70 vol% CH_3OH solution at voltage of 20 V and −30 °C. The EBSD measurements were carried out by the use of FE-SEM produced by FEI attached with the EBSD measurement system produced by TSL at an accelerate voltage of 15 kV. The step size used in the EBSD measurements was 50 nm.

For TEM observations, the specimens perpendicular to TD of the sheet were mechanically polished to 50-μm thickness and then electro-polished in the same solution under the same condition as preparation for the EBSD specimen. TEM observations were carried out with Hitachi H-800 operated at 200 kV.

Table 1 Chemical composition of the specimen studied (mass%)

Si	Fe	Cu	Mg	Ti	Al
0.01	0.61	0.14	0.01	0.01	99.11

Results

Change in mechanical properties of the ARB-processed specimens by annealing and subsequent deformation

Figure 1a shows nominal stress–strain curves of the 6-cycle ARB-processed specimens. The horizontal axis indicates the nominal plastic strain, after extracting the elastic component. The stress–strain curve of the 6-cycle ARB-processed specimen showed the peak stress at strain of 2.8%, indicating limited uniform elongation. The shape of the curve is typical for the UFG aluminum fabricated by the ARB [7]. The flow stress decreased by 150 °C annealing and increased by the subsequent deformation by 15% cold-rolling. That is, the "hardening by annealing and softening by deformation" phenomena did not happen, but the change in the stress–strain behaviors was the typical ones in the conventionally coarse-grained materials. The shape of the stress–strain curves did not greatly change by annealing and subsequent deformation, though the total elongation decreased by about 5%.

The nominal stress–strain curves of the 10-cycle ARB-processed specimens were shown in Fig. 1b. The shape of the curve for the 10-cycle ARB-processed specimen was similar to that for the 6-cycle specimen, though the tensile strength increased from 251 to 293 MPa. The shape of the stress–strain curve for the annealed 10-cycle ARB specimen was quite different from that for the as-ARB specimen. In the annealed specimen, the strength at early stage of tensile test slightly increased and the elongation greatly decreased. Furthermore, the strain at the peak stress shifted to lower side after annealing. The flow stress of the as-ARB specimen decreased monotonously and after the peak stress, while the flow stress of the annealed specimen

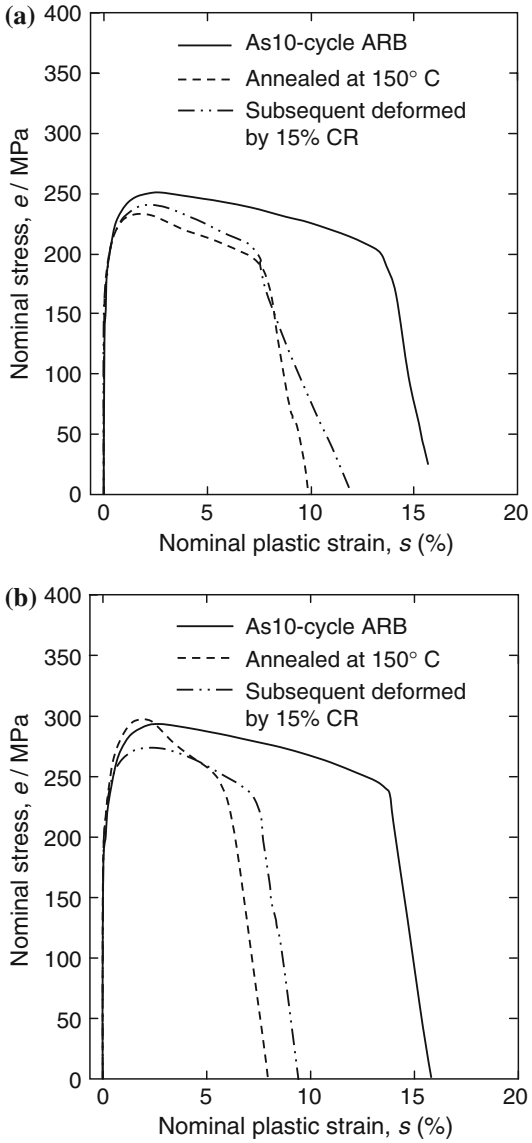

Fig. 1 The nominal stress–strain curves of the (**a**) 6-cycle ARB-processed specimens and (**b**) 10-cycyle ARB-processed specimens. The curves for the specimens annealed at 150 °C for 1.8 ks after the ARB and for the specimens subsequently deformed by 15% cold-rolling after the 150 °C annealing were also shown in the figures

showed an unique shape having an inflection after the peak stress. By the subsequent deformation, the strength significantly decreased and the total elongation increased, that is, the peculiar phenomena happened in the 10-cycle ARB-processed specimens.

The ultimate tensile strength (σ_B), 0.2% proof stress ($\sigma_{0.2}$), uniform elongation (e_u), and total elongation (e_t) of the various specimens were summarized in Table 2. In the 6-cycle specimens, the tensile strength decreased by annealing and increased by deformation. The 0.2% proof stress did not change so much by annealing and subsequent deformation. On the other hand, in the 10-cycle specimens, both the tensile strength and 0.2% proof stress increased by annealing and decreased by deformation, which confirmed the occurrence of the "hardening by annealing and softening by deformation" phenomena only in the 10-cycle specimen. The tensile test for the 10-cycle specimen was repeated two times and reproducible result was obtained. Therefore, it can be concluded that the occurrence of the peculiar phenomena depends on the applied strain in the ARB process.

Microstructure of the ARB-processed and annealed specimens

Figure 2 shows the grain boundary maps obtained from the EBSD measurements for the ARB-processed and 150 °C annealed specimens. In the figures, high-angle grain boundaries with misorientation angle larger than 15° are drawn in green lines, while boundaries with misorientation angle between 2 and 15° in red lines. The microstructures of all the specimens showed the ultrafine lamellar boundary structure [8] elongated to RD.

The microstructural parameters obtained from the EBSD results were summarized in Table 3. The mean spacing of high-angle lamellar boundaries (d_{HABG}) were 280, 340, 190, and 250 nm for the 6-cycle specimen, 6-cycle + 150 °C annealed specimen, 10-cycle specimen, and 10-cycle + 150 °C annealed specimen, respectively. The mean lamellar spacing in the 6-cycle specimens was larger than that in the 10-cycle specimen. By annealing, the mean spacing increased slightly in both specimens, which indicates the microstructure coarsening by grain boundary migration during annealing. The fraction of high-angle boundaries (f_{HAGB}) was ~70% for all specimens. The difference in f_{HAGB} between the as-6-cycle specimen and

Table 2 Mechanical properties of the ARB-processed specimens

Specimens	σ_B (MPa)	$\sigma_{0.2}$ (MPa)	e_u (%)	e_t (%)
6-cycle ARB	251	199	2.73	15.8
6-cycle ARB + 150 °C annealing	233	192	1.74	10.0
6-cycle ARB + 150 °C annealing + 15% cold-rolling	240	187	2.28	12.0
10-cycle ARB	293	218	2.89	16.0
10-cycle ARB + 150 °C annealing	298	231	1.94	8.14
10-cycle ARB + 150 °C annealing + 15% cold-rolling	274	228	2.35	9.49

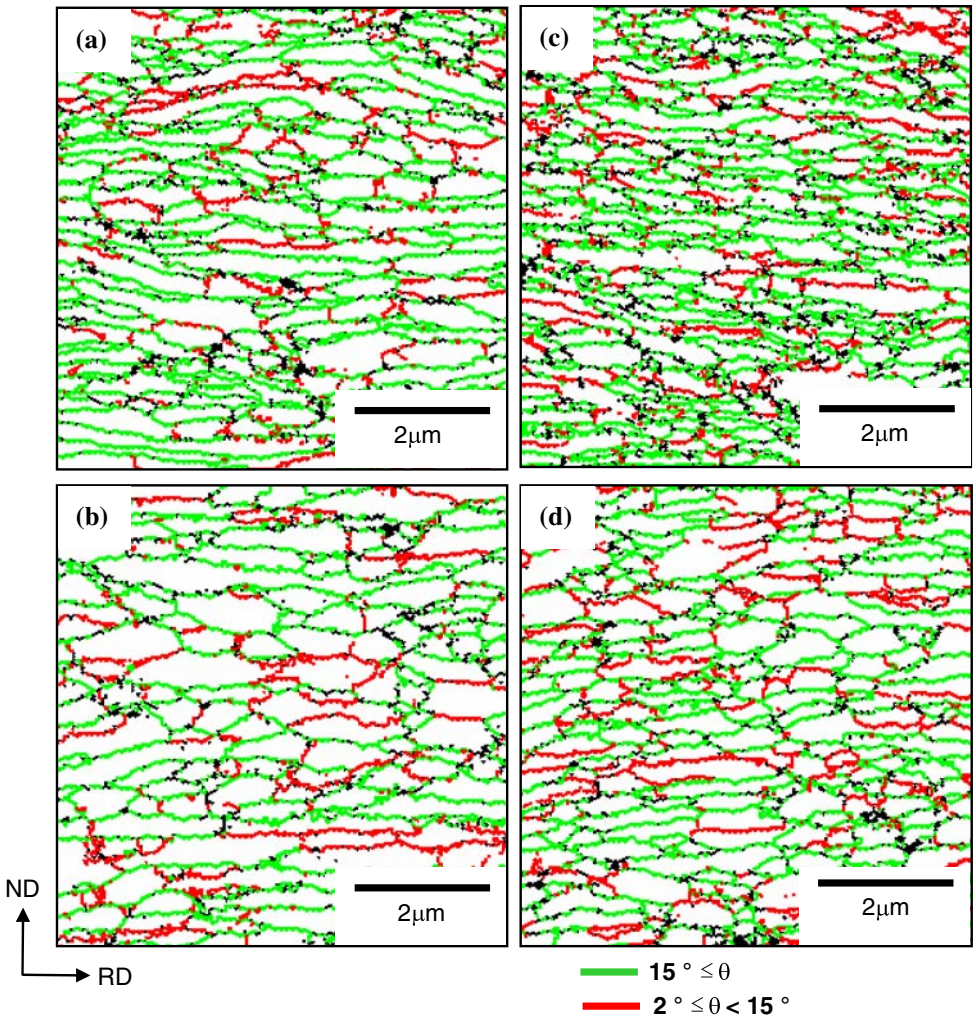

Fig. 2 The grain boundary maps obtained from the EBSD measurements for the various specimens. (**a**) 6-cycle ARB-processed. (**b**) 6-cycle ARB-processed and 150 °C annealed. (**c**) 10-cycle ARB-processed. (**d**) 10-cycle ARB-processed and 150 °C annealed

Table 3 Microstructural parameters obtained from the EBSD analysis of the ARB-processed specimens

Specimens	d_{HAGB} (nm)	d_{All} (nm)	f_{HAGB} (%)
6-cycle ARB	280	260	69
6-cycle ARB + 150 °C annealing	340	280	68
10-cycle ARB	190	180	71
10-cycle ARB + 150 °C annealing	250	200	67

the as-10-cycle specimen was <2%. The fraction hardly changed after annealing in both specimens.

Figure 3 shows TEM microstructures of the ARB-processed and annealed specimens. The lamellar boundary structures elongated to RD were observed in all the specimens. The spacing of the lamellar varied from several tens of nanometers to several hundreds of nanometers. The mean lamellar spacing for the 6-cycle specimen, 6-cycle + 150 °C annealed specimen, 10-cycle specimen, and 10-cycle + 150 °C annealed specimen was 250, 260, 210, and 230 nm, respectively. These values agreed well with the mean spacing of all boundaries (d_{All}) obtained from the EBSD measurements. In Fig. 3, it was seen that the dislocation density in the annealed 10-cycle specimen was relatively lower than that in the annealed 6-cycle specimen. Many grains having dislocation tangles were observed in the annealed 6-cycle specimen even after annealing. In the case of the 10-cycle specimen, the dislocation tangles were significantly annihilated by annealing (Fig. 3d).

Discussion

Difference in microstructures between 6-cycle ARB and 10-cycle ARB

From the present results, it was found that the amount of strain applied in the ARB process greatly affects the occurrence of the "hardening by annealing and softening by deformation" phenomena. The peculiar phenomena did

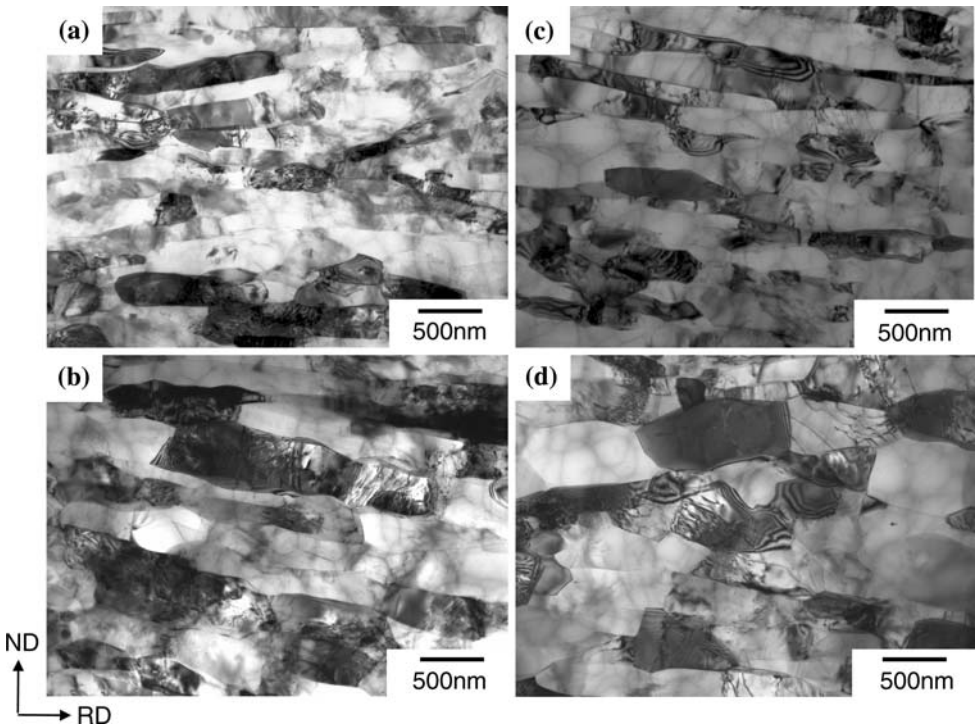

Fig. 3 The TEM microstructures for the various specimens. (**a**) 6-cycle ARB-processed. (**b**) 6-cycle ARB-processed and 150 °C annealed. (**c**) 10-cycle ARB-processed. (**d**) 10-cycle ARB-processed and 150 °C annealed

not occur in the 6-cycle ARB-processed specimens but happened in the 10-cycle ARB-processed specimens. The 6-cycle specimen was softened by annealing and hardened by deformation normally, although the 1100-Al ARB-processed by six cycles without lubrication exhibited the peculiar phenomena in the previous study [5]. In the 1100-Al ARB-processed without lubrication, the thickness of lamellar and fraction of high-angle boundary were 180 nm and 66.3%, respectively. After annealing, the thickness of lamellar and fraction of high-angle boundary changed to 225 nm and 63.9%, respectively [5]. These microstructural parameters were quite similar to that of the present specimen ARB-processed by 10-cycle with lubrication. Thus, the difference is considered to be caused by the difference in the structural parameters between the 6-cycle and the 10-cycle samples. Especially, the difference in the microstructures after annealing is important because the "hardening by annealing" is expected to be attributed to the annihilation of free dislocations and dislocation sources during annealing [5]. In the case of the "softening by deformation," the introduction of free dislocations as well as activated dislocation sources is thought to make the plastic deformation of the UFG polycrystals easier. Thus, the structural parameters of the annealed materials were compared based on the quantitative data obtained in this study.

One of the important structural parameters is the dislocation density within the grains, because the "hardening by annealing" is caused by the deficiency of free mobile dislocations. From the TEM observation, it was seen that the dislocation density in the annealed 6-cycle specimen was higher than that in the annealed 10-cycle specimen. Additionally, the dislocation tangles observed in the annealed 6-cycle specimen probably work as dislocation sources. These agree with the experimental result that the peculiar phenomena did not happen in the 6-cycle specimens. One of the reasons for the difference in the dislocation density is considered to be the difference in the grain size. Annihilation of dislocations is probably easier in the smaller grain size, since the grain boundaries can act as sink for dislocations and the substantial diffusivity is high in the finer grain size owing to boundary diffusion.

The effect of crystal orientation is another possible cause of the difference in the dislocation density. It was known that the deformed microstructure, including dislocation density within the grains, depends on the crystal orientation [9, 10]. Lubrication condition significantly affects the texture of ARB-processed sheets, because redundant shear strain is introduced in subsurface regions under high friction conditions [11]. Table 4 shows the fractions of typical rolling texture components [12] in the annealed 6-cycle and 10-cycle specimens. For comparison, the texture components in the annealed 1100-Al ARB-processed by 6-cycles without lubrication was also shown in Table 4. It was found that the copper orientation increased and the brass orientation decreased as the ARB strain increased in the specimens ARB-processed with lubrication. The brass component of the specimens ARB-processed without lubrication was almost same as that of the 10-cycle specimen. If the dislocation annihilation is

Table 4 Fraction of the typical rolling textures in the annealed 6-cycle specimen with lubrication, the annealed 10-cycle specimen with lubrication, and the annealed 6-cycle specimen without lubrication obtained from the EBSD analysis

Specimen	{112}<111> Copper (%)	{110}<112> Brass (%)	{123}<634> S (%)
6-cycle ARB + 150 °C annealing	16	21	45
10-cycle ARB + 150 °C annealing	33	7.2	37
6-cycle ARB without lubrication + 150 °C annealing	14	7.9	15

difficult, or the dislocation multiplication is easy in the grains with the brass orientation, the peculiar phenomena would be inhibited in the 6-cycle specimen (with lubrication).

Because low-angle boundaries having misorientation angles <15° are considered to be composed of dislocation arrays, they are expected to work as dislocation sources in deformation [13]. Thus, another important microstructural parameter is the fraction of low-angle boundaries in the microstructures. A distance between adjacent dislocations in the dislocation arrays (or a distance of the nodes in the dislocation networks) increases with decreasing the misorientation of the boundary. Because the stress to bow-out a dislocation is in inverse proportion to the distance between dislocations, the dislocation sources might be activated on the boundary having very low-angle misorientation. Therefore, the fraction of very low-angle boundaries is important. However, the misorientation <2° is not resolved by the EBSP measurement. Thus, the present boundary data obtained from the EBSP measurement is not enough to discuss the low-angle boundary as a dislocation source. The TEM/Kikuchi-line analysis, which can distinguish very low-angle boundaries, is needed to discuss this parameter in future.

Though the substantial SPD strain applied in the present specimen ARB-processed by 10-cycle with lubrication is different from that in the 6-cycle specimen without lubrication in the previous study [5], because of the redundant shear strain in the case of non-lubricated ARB, both specimens showed the similar microstructure and exhibited the "hardening by annealing and softening by deformation" phenomena. Therefore, it is consequently concluded that the grain size and texture components that depend on the amount of the applied SPD strain and the rolling conditions are considered to be important for the appearance of the peculiar phenomena.

Conclusions

The peculiar phenomena in the UFG Al, "hardening by annealing and softening by deformation," were investigated in details using the commercial purity aluminum ARB-processed by six or ten cycles with good lubrication. The main results are summarized below:

1. The 10-cycle ARB-processed specimens showed the "hardening by annealing and softening by deformation" phenomena. On the other hand, the 6-cycle ARB-processed specimens did not show the unique phenomena but were softened by annealing and hardened by deformation normally.
2. The mean spacing of the lamellar boundaries in the 6-cycle specimens was slightly smaller than that in the 10-cycle specimens. Both specimens showed the same fraction of high-angle boundaries, which was ~70%.
3. It was confirmed that the dislocation density in the annealed 6-cycle specimen was higher than that in the annealed 10-cycle specimen. The difference in the dislocation density was suggested to result in the occurrence of the peculiar phenomena.

Acknowledgements This study was financially supported by the Global COE Program (Center of Excellence for Advanced Structural and Functional Materials Design) in Osaka University and the Grant-in-Aid for Scientific Research on the Priority Area "Giant Straining Process for Advanced Materials Containing Ultra-High Density Lattice Defects," both through the Ministry of Education, Culture, Sports, Science and Technology (MEXT), Japan.

References

1. Langdon TG (2007) Mater Sci Eng A 462:3. doi:10.1016/j.msea.2006.02.473
2. Islamgaliev RK, Yunusova NF, Sabirov IN, Sergueeva AV, Valiev RZ (2001) Mater Sci Eng A 319:877. doi:10.1016/S0921-5093(01)01052-8
3. Tsuji N, Saito Y, Lee SH, Minamino Y (2003) Adv Eng Mater 5:338. doi:10.1002/adem.200310077
4. Song R, Ponge D, Raabe D, Speer JG, Matlock DK (2006) Mater Sci Eng A 441:1. doi:10.1016/j.msea.2006.08.095
5. Huang X, Hansen N, Tsuji N (2006) Science 312:249. doi:10.1126/science.1124268
6. Huang X, Kamikawa N, Tsuji N, Hansen N (2008) ISIJ Int 48:1080
7. Tsuji N, Ito Y, Sato Y, Minamino Y (2002) Scripta Mater 47:893. doi:10.1016/S1359-6462(02)00282-8
8. Hansen N, Jensen DJ (1999) Philos Trans R Soc Lond A 357:1447. doi:10.1098/rsta.1999.0384
9. Huang X, Hansen N (1997) Scripta Mater 317:1. doi:10.1016/S1359-6462(97)00072-9

10. Hansen N, Huang X (1998) Acta Mater 46:1827. doi:10.1016/S1359-6454(97)00365-0
11. Kamikawa N, Tsuji N, Huang X, Hansen N (2007) Mater Trans 48:1978. doi:10.2320/matertrans.MA200702
12. Humphreys FJ, Hatherly M (1995) Recrystallization and related annealing phenomena. Pergamon, UK
13. Fujita H, Yamada H (1970) J Phys Soc Jpn 29:132. doi:10.1143/JPSJ.29.132